Biosensors and Bioelectronics 129 (2019) 72–78

Contents lists available at ScienceDirect

Biosensors and Bioelectronics

journal homepage: www.elsevier.com/locate/bios

Electrochemiluminescence energy resonance transfer in 2D/2D heterostructured g-C_3N_4/MnO_2 for glutathione detection

Xiao-Long Fu[a], Fang Hou[a], Fu-Rao Liu[a], Shu-Wei Ren[b], Jun-Tao Cao[a,*], Yan-Ming Liu[a,*]

[a] College of Chemistry and Chemical Engineering, Institute for Conservation and Utilization of Agro-bioresources in Dabie Mountains, Xinyang Normal University, Xinyang 464000, China

[b] Xinyang Central Hospital, Xinyang 464000, China

ARTICLE INFO

Keywords:
Electrochemiluminescence resonance energy transfer
2D/2D heterostructured g-C_3N_4/MnO_2
Glutathione

ABSTRACT

The energy transfer efficiency, strongly depending on the distance of donor–acceptor pair, is always a crucial factor for the construction of elegant electrochemiluminescence resonance energy transfer (ECL-RET)-based biosensors. In this paper, a novel and efficient ECL-RET in 2D/2D heterostructured g-C_3N_4/MnO_2 was developed using g-C_3N_4 nanosheets (g-C_3N_4 NSs) as energy donor and MnO_2 nanosheets (MnO_2 NSs) as energy acceptor. In this system, MnO_2 NSs in-situ grew on g-C_3N_4 NSs to form the 2D/2D heterostructure, greatly shortening the distance of the donor–acceptor pair (g-C_3N_4–MnO_2) and thus greatly enhancing the RET efficiency. To demonstrate the performance of the system, a signal "off-on" ECL sensor was designed for glutathione (GSH) analysis. In the absence of GSH, MnO_2 significantly quenched the ECL intensity of g-C_3N_4 owing to ECL-RET in this 2D/2D g-C_3N_4/MnO_2 heterostructure (ECL signal "off"). Upon the addition of GSH, MnO_2 was reduced to Mn^{2+} by GSH and g-C_3N_4 was released from the heterostructured g-C_3N_4/MnO_2, generating a recovery of ECL intensity (ECL signal "on"). Under the optimal conditions, the designed ECL-RET signal "off-on" sensor realized the sensitive detection of GSH ranged from 0.2–100 μM with the detection limit of 0.05 μM. Furthermore, the as-prepared ECL-RET sensor exhibits good performance in the determination of GSH in human serum samples. The ECL-RET in 2D/2D heterostructure provides an ingenious way for the exploitation of novel ECL biosensing systems.

1. Introduction

Electrochemiluminescence (ECL) detection with high sensitivity, low background signal, broad dynamic response range and simplified optical setup has attracted increasing attentions in bioanalysis (Cao et al., 2018; Zhang et al., 2018; Wang et al., 2018). As one of the most interesting protocols to enhance the ECL response, ECL resonance energy transfer (ECL-RET) has been witnessed to be the effective signaling mechanism to develop the highly sensitive and specific ECL biosensing system (Dong et al., 2014; Ji et al., 2014). The essential prerequisite in ECL-RET system is the perfect overlap of emission spectrum of donor and absorption spectrum of acceptor as well as the close proximity (less than 10 nm) between the donor and acceptor (Ji et al., 2016; Wang et al., 2011). In the past few years, the researchers have devoted to initiating the suitably matched ECL-RET donor–acceptor pairs and establishing various ECL-RET sensing platforms for the analysis of protein (Liu et al., 2015; Ke et al., 2018), RNA (Hao et al., 2014; Peng et al., 2017) and some ions (Babamiri et al., 2018; Lei et al., 2015). For instance, on the basis of RuSi@$Ru(bpy)_3^{2+}$ and Au@Ag_2S, Xu's group (Wu et al., 2014) employed an ECL-RET system for DNA detection. Wei's group (Ma et al., 2016) reported $Ru(bpy)_3^{2+}$/Au nanoparticle-doped Pb(II)-β-cyclodextrin ECL-RET sensor for insulin detection. In those systems, the donor–acceptor pair was normally independent, separated by the appropriate antigen-antibody or the specific length aptamer strand. Nevertheless, the efficiency of ECL-RET is strongly relied on the distance between the donor and acceptor. The comparative long path of energy transfer between donor and acceptor based on antigen-antibody or aptamer strand could lead to energy loss and reduce ECL-RET efficiency, which enormously impede the further progress of ECL-RET. To break through the hindrance, the latest researches proved that the combination of donor and acceptor into a nanomaterial can obviously reduce the energy loss and effectively boost the efficiency (Li et al., 2017; Chen et al., 2018). Such ECL-RET strategy in one nanostructure will provide an ingenious way for designing sensitive ECL biosensors and hold broad prospect for expanding the applications of ECL technique. Yet, this method is still in its infancy, exploring the

* Corresponding authors.
E-mail addresses: jtcao11@163.com (J.-T. Cao), liuym9518@sina.com (Y.-M. Liu).

https://doi.org/10.1016/j.bios.2019.01.010
Received 23 October 2018; Received in revised form 30 December 2018; Accepted 3 January 2019
Available online 15 January 2019
0956-5663/

novel system for ECL bioanalysis is desirable.

Graphitic-phase C_3N_4 nanosheets (g-C_3N_4 NSs), as a fascinating ECL emitter, amaze the researchers in virtue of their high quantum yields, stable chemical properties and nontoxicity (Wang et al., 2016; Liu et al., 2014; Feng et al., 2015). These advantages allow them particularly popular in different types of ECL sensors. Two-dimensional (2D) manganese dioxide nanosheets (MnO_2 NSs) have been recognized as a class of nanomaterials with facile-synthesized, good biocompatibility and physicochemical properties, which display an intense absorption in the wide ultraviolet-visible region from 280 nm to 600 nm (Sakai et al., 2005; Yuan et al., 2014; Yu and Zheng, 2016). Coincidentally, the emission spectrum of g-C_3N_4 NSs centers at 435 nm, overlapping well with absorption spectrum of MnO_2 NSs, which makes them a suitable donor–acceptor pair for the ECL-RET.

Glutathione (GSH), a ubiquitous biologic mercaptan, possesses an important relation with scavenging toxins and free radicals, maintaining redox homeostasis, and involving in gene regulation (Chen et al., 2015; Harfield et al., 2012; Sezgintürk and Dinçkaya, 2004). The abnormal level of GSH may act as a trigger for many diseases typically implicated in cancer, liver damage, HIV, aging, Parkinson, and others (Ngamchuea et al., 2017; Niu et al., 2015; Yin et al., 2014). Therefore, the measurement and quantification of GSH holds promising biological and clinical significance and has become the important research subject, which gains great concerns of the researchers. Innovatively, due to the unique redox reaction between MnO_2 and GSH ($MnO_2 + 2GSH + 2H^+ = Mn^{2+} + GSSG + 2H_2O$), MnO_2 NSs could serve as recognition units for the detection of GSH, which has been rarely reported in the field of ECL detection.

Herein, a high-efficient ECL-RET strategy by integrating g-C_3N_4 NSs (the donor) and MnO_2 NSs (the acceptor) into one nanostructure was developed for GSH detection. The 2D/2D heterostructured g-C_3N_4/MnO_2 was prepared by in-situ reduction of MnO_4^- on g-C_3N_4 NSs. The compact contact between g-C_3N_4 and MnO_2 shortened the distance of the donor–acceptor pair (g-C_3N_4–MnO_2) and generated an enhanced RET, contributing to a significantly quenched ECL of g-C_3N_4. To demonstrate the proof-of-concept of the system, an ECL "off-on" sensing platform was fabricated and the schematic principle is illustrated in Scheme 1. In the absence of GSH, the efficient RET between g-C_3N_4 and MnO_2 in this heterostructure produced a very weak ECL emission (ECL signal "off"). The addition of GSH could decompose the MnO_2 NSs by the redox reaction between GSH and MnO_2, enabling the recovery of ECL intensity of g-C_3N_4 NSs (ECL signal "on"). The efficient ECL-RET in this 2D/2D heterostructured g-C_3N_4/MnO_2 endows the ECL sensor for GSH detection with high sensitivity. The as-proposed ECL sensor had been successfully applied for the practical application with the excellent analytical performance.

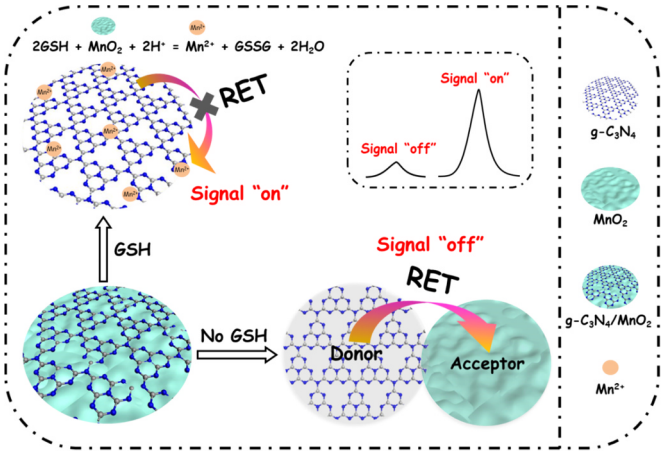

Scheme 1. Schematic principle of the designed "off-on" ECL-RET sensing platform for GSH detection.

2. Experimental

2.1. Materials and reagents

Melamine, GSH, homocysteine (Hcy) and L-cysteine (Cys) were obtained from Aladdin Industrial Co., Ltd. (Shanghai, China). 2-(N-morpholino) ethanesulfonic acid (MES) and glycine (Gly) were purchased from Shanghai Seebio Biotechnology, Inc. (Shanghai, China). L-serine (Ser), L-lysine (Lys), potassium permanganate ($KMnO_4$), zinc sulfate ($ZnSO_4$), cupric sulfate ($CuSO_4$), ferrous sulfate ($FeSO_4$), ferric chloride ($FeCl_3$), calcium chloride ($CaCl_2$), nitric acid (HNO_3), potassium persulfate ($K_2S_2O_8$), ascorbic acid (AA), citrate acid (CA) and 36% acetic acid were from Sinopharm Chemical Reagent Co., Ltd. (Shanghai, China). Glucose, sucrose and magnesium chloride ($MgCl_2$) were from Tianjin Yongda Chemical Reagent Co., Ltd. (Tianjing, China). Phosphate buffered solution (PBS, pH 7.4, 0.1 M) containing NaH_2PO_4, K_2HPO_4, KCl and NaCl was used as the electrolyte. All reagents were of analytical reagent grade.

2.2. Apparatus

ECL signals were taken by a MPI-B ECL analyzer coupled with a multifunctional chemiluminescence detector (Xi'An Remax Electronic Science & Technology Co., Ltd., Xi'An, China). In ECL measurements, modified glassy carbon electrode (GCE, 5 mm in diameter) as the working electrode, Ag/AgCl electrode as the reference electrode, and platinum electrode as the counter electrode were used. Scanning electron microscopy (SEM) images and transmission electron microscope (TEM) images were recorded on S 4800 (Hitachi, Tokyo, Japan) and Tecnai G2 F 20 TEM system (FEI Co., Ltd., USA), respectively. Dynamic light scattering (DLS) measurements were carried out on a Zetasizer Nano ZS (Malven, UK). Ultraviolet-visible (UV–vis) absorption spectrum was obtained by a Shimadzu UVmini-1240 UV–vis spectrophotometer (Kyoto, Japan). Fluorescence (FL) spectra were acquired by the Hitachi F-7000 spectrofluorophotometer (Kyoto, Japan).

2.3. Synthesis of g-C_3N_4 NSs

The preparation of g-C_3N_4 NSs was conducted by a previously reported method with slight modifications (Zhang et al., 2012; Tian et al., 2013; Chen et al., 2013). First, the yellow bulk g-C_3N_4 was obtained via calcination of melamine. Briefly, 5 g white melamine powers were annealed at 550 °C for 4 h. Second, g-C_3N_4 nanoflakes were produced by chemically oxidizing the products from the first step with HNO_3. In brief, 300 mg above obtained products ground to powder were put into 100 mL of HNO_3 (5 M) and the mixture was subjected to ultrasound for 1 h. Subsequently, the solution was refluxed for 12 h at 125 °C. Till it cooled, the refluxed products were centrifuged and washed to neutral. Finally, the ultrathin g-C_3N_4 NSs were from the liquid exfoliation of as-prepared nanoflakes. As following, the g-C_3N_4 nanoflakes from the previous step were exfoliated in 30 mL water by performing a sonication for 16 h constantly. Further, the results were centrifuged to remove unexfoliated g-C_3N_4. The collected suspension was g-C_3N_4 NSs solution.

2.4. Synthesis of 2D/2D heterostructured g-C_3N_4/MnO_2

The 2D/2D heterostructured g-C_3N_4/MnO_2 was prepared according to the literature (Zhang et al., 2014). 0.25 mL g-C_3N_4 NSs, 1 mL 10 mM $KMnO_4$ solution and 6.25 mL water were added to 2.5 mL 0.1 M MES (pH 6.0) buffer solution in turn. Afterwards, a sonication was performed on the mixture until the solution turned to a brown colloid. The g-C_3N_4/MnO_2 was gathered by centrifuging and purified by rinsing with water. The obtained precipitates were dispersed into 10 mL water for further use. Similar to the method above, MnO_2 NSs were prepared without g-C_3N_4 addition.

2.5. ECL measurements of 2D/2D heterostructured g-C_3N_4/MnO_2

For the ECL measurements of g-C_3N_4/MnO_2, the detection solution contained 50 μL g-C_3N_4/MnO_2, 50 μL water and 5 mL PBS with 0.1 M $K_2S_2O_8$. The ECL signals were carried out with working potential varied between −1.6 and 0 V, a scanning rate of 0.1 V s^{-1} and the voltage of photomultiplier tube (PMT) set at 800 V, which was through the whole experiment.

2.6. Procedure of GSH detection

To explore the ECL sensing detection of GSH solution, 50 μL GSH of different concentrations were thoroughly vortex-mixed with 50 μL g-C_3N_4/MnO_2 for 10 min reaction at room temperature. Subsequently, the mixture was transferred into 5 mL PBS containing 0.1 M $K_2S_2O_8$ for subsequent ECL measurement.

2.7. Selectivity of GSH detection

For examining the selectivity of ECL assay towards GSH, some different electrolytes and biomolecules including KCl, $MgCl_2$, $CaCl_2$, $ZnSO_4$, $CuSO_4$, $FeSO_4$, $FeCl_3$, glucose, sucrose, CA, Gly, Lys, Ser (each of 1 mM), Hcy, Cys, AA (each of 10 μM) and GSH (100 μM) were prepared. Similarly, 50 μL of the prepared samples reacted with 50 μL g-C_3N_4/MnO_2 for 10 min at room temperature, respectively. After being mixed with 5 mL PBS containing 0.1 M $K_2S_2O_8$, ECL spectra were detected.

2.8. Application of ECL sensor for serum samples analysis

To investigate the applicability of the sensing strategy in clinical analysis, the GSH in human serum samples were examined. The human serum samples from Xinyang Central Hospital were pretreated as follows: 250 μL human serum samples, 250 μL of 1.2 M acetic acid and 20 mg zinc powder were incubated for 1 h at 37 °C under shaking. The products were centrifuged and the suspensions were collected. Consequently, total GSH in serum was the sum of the intrinsic GSH and generated GSH from the oxidized form GSSH by zinc powder. Then, the mixtures of 50 μL pretreated human serum samples with 100-fold dilution and 50 μL g-C_3N_4/MnO_2 were vigorously shook and introduced into 5 mL PBS containing 0.1 M $K_2S_2O_8$. And the ECL signals were recorded.

3. Results and discussion

3.1. Characterization of 2D/2D heterostructured g-C_3N_4/MnO_2

The successful preparation of nanomaterial is vital for construction of an efficient and sensitive ECL sensing platform. In this work, to obtain 2D/2D heterostructured g-C_3N_4/MnO_2, MnO_4^- was in-situ reduced to g-C_3N_4 NSs in the presence of MES buffer. As an essential raw material, the concentration of $KMnO_4$ was directly correlative with the morphology and property of g-C_3N_4/MnO_2. Therefore, we firstly optimized the concentration of $KMnO_4$ by ECL and FL measurement. As expected in Fig. 1A, the ECL signals of g-C_3N_4/MnO_2 declined with the $KMnO_4$ concentration increasing until 5 mM. The ECL intensity showed no obvious change with $KMnO_4$ concentration over 5 mM. Furthermore, the FL spectrum (Fig. 1B) of g-C_3N_4/MnO_2 was obtained with the similar signal variation process. Taking account of ECL and FL analysis, 5 mM $KMnO_4$ was chose to form 2D/2D heterostructured g-C_3N_4/MnO_2 and used for subsequent experiments.

SEM and TEM were used to depict the morphology of as-prepared 2D/2D heterostructure. Fig. 2A indicates that the exfoliated g-C_3N_4 NSs present a layered 2D structure. MnO_2 NSs exhibit a large 2D lamellar morphology with irregular stacking wrinkles (Fig. 2B). Comparison with Fig. 2A and B, the thin layered structure of g-C_3N_4 and the ultrathin lamellar morphology of MnO_2 were perfectly expressed in the Fig. 2C (the SEM image of g-C_3N_4/MnO_2), which suggested that MnO_2 NSs were successfully decorated on the surface of g-C_3N_4 NSs. TEM, HRTEM and mapping images further illustrate the successful synthesis of g-C_3N_4/MnO_2. From the TEM image of g-C_3N_4/MnO_2 (Fig. 2D), the gauzy MnO_2 and the layered g-C_3N_4 could be clearly distinguished. The HRTEM image (Fig. 2E) shows a close integration between MnO_2 and g-C_3N_4 to form this 2D/2D heterostructured morphology. The dark strips corresponded to the multiple folds and crinkles of MnO_2 NSs. Meanwhile, the clear lattice fringes with a lattice spacing of 0.24 nm of MnO_2 NSs were observed from the HRTEM image (Fig. 2F). The EDX elemental mapping images (Fig. 2G-I corresponding to Fig. 2D) verify the coexistence of N, O, Mn elements in this heterostructure.

Furthermore, DLS was also used for characterizing the size of g-C_3N_4, MnO_2, and the prepared g-C_3N_4/MnO_2. As displayed in Fig. S1, after MnO_2 in-situ grew on the g-C_3N_4 to form g-C_3N_4/MnO_2 (blue curve), the size greatly increased compared with the single g-C_3N_4 (black curve) and MnO_2 (red curve), revealing the successful combination of g-C_3N_4 and MnO_2.

3.2. ECL-RET in the 2D/2D heterostructured g-C_3N_4/MnO_2

To substantiate the existence of the ECL-RET between g-C_3N_4 and MnO_2 in g-C_3N_4/MnO_2, the emission spectrum of g-C_3N_4 NSs and absorption spectrum of MnO_2 NSs were studied. As depicted in Fig. 3A, the emission spectrum of g-C_3N_4 NSs centered at 435 nm, and the absorption spectrum of MnO_2 NSs expressed a wide and intense absorption band from 280 nm to 600 nm, displaying the perfect overlap between these spectra. This overlap ensured the feasibility of the ECL-RET process. Subsequently, the ECL-RET process was further proved by ECL experiments. The g-C_3N_4 NSs showed a strong ECL signal (Fig. 3B, curve 1), while a remarkable decline was observed after depositing MnO_2 on g-C_3N_4 (Fig. 3B, curve 4), indicating that the highly efficient RET occurred between g-C_3N_4 and MnO_2.

The signaling process could be deduced as follows. In the absence of MnO_2, g-C_3N_4 was excited to g-$C_3N_4^*$ undergoing electrochemical redox reaction (Cheng et al., 2012). The strong ECL emission is generated during return process of the excited state of g-C_3N_4 to the ground state. In the presence of MnO_2, the excited state energy of g-$C_3N_4^*$ was partly migrated to the closely contacted MnO_2 during the return process of the excited state, causing the decay of the ECL emission. That was why MnO_2 triggered the quenching of the g-C_3N_4 ECL response.

To study the RET efficiency, a series of g-C_3N_4/MnO_2 heterostructures were prepared with varied growth time of MnO_2 on g-C_3N_4, and the ECL responses of g-C_3N_4/MnO_2 heterostructures were investigated. As shown in Fig. S2A, with the time of the in-situ growth of MnO_2 increased, the ECL intensity gradually decreased until 30 min. The reaction time longer than 30 min did not result in further signal decrement. The corresponding RET efficiency was determined according to the literatures (Clapp et al., 2004; Qian et al., 2013),

$$E = 1 - F_{DA}/F_D$$

where E is the RET efficiency, F_{DA} is the ECL intensity of the donor (g-C_3N_4) in the presence of the acceptor (MnO_2), and F_D is the ECL intensity of the donor (g-C_3N_4) alone. As shown in Fig. S2B, with the time of in-situ growth of MnO_2 increased, the RET efficiency increased and then reached maximum at the time point of 30 min.

For further verifying that the in-situ growth of MnO_2 benefited to the efficiency of RET, the ECL behavior of g-C_3N_4 by directly adding MnO_2 solution into g-C_3N_4 solution was also recorded. As illustrated in Fig. S2C, the g-C_3N_4 solution generated a strong ECL peak of 2245 a.u. (curve a). When MnO_2 solution was directly added into g-C_3N_4 solution, a decreased ECL intensity about 1386 a.u. was obtained (curve b). The RET efficiency was calculated to be 38.26%. While the MnO_2 in-situ grew on g-C_3N_4 to form one nanostructure, the lower ECL intensity of 278 a.u. was observed (curve c). The RET efficiency of the in-situ growth of MnO_2 was greatly improved to be 87.62%, indicating the high-efficient ECL-RET occurred in g-C_3N_4/MnO_2 heterostructure.

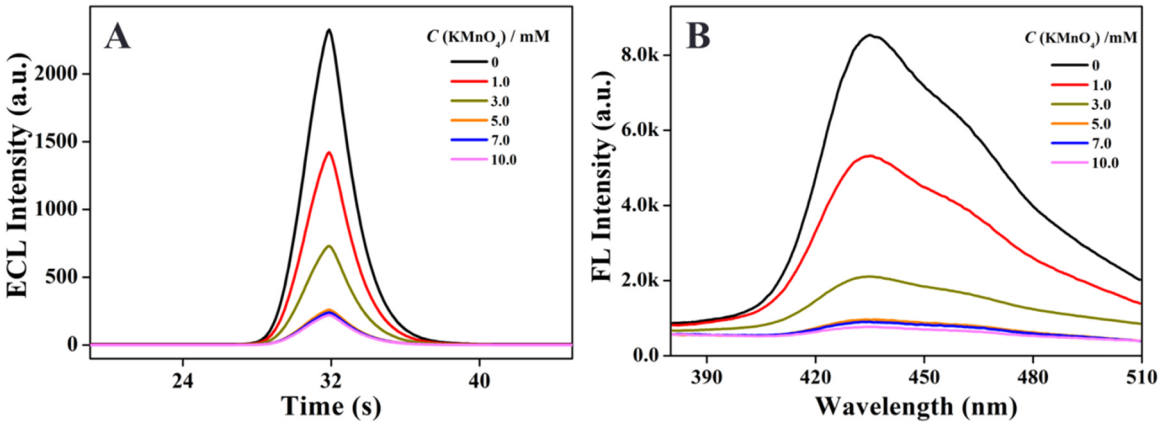

Fig. 1. ECL (A) and FL (B) intensity of 2D/2D heterostructured g-C_3N_4/MnO_2 using different concentrations of $KMnO_4$.

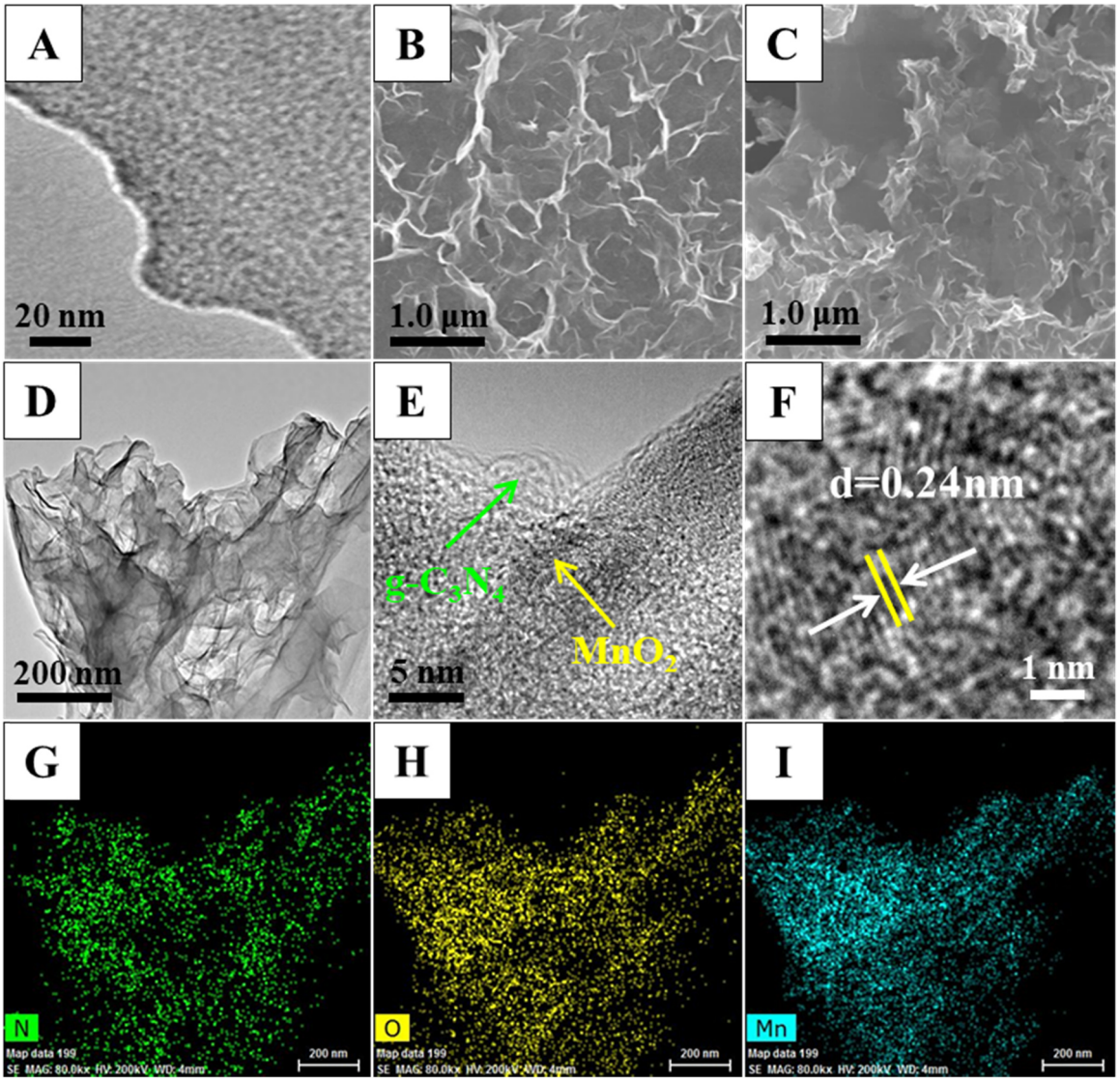

Fig. 2. TEM image of g-C_3N_4 NSs (A), SEM image of MnO_2 NSs (B), SEM image of 2D/2D heterostructured g-C_3N_4/MnO_2 (C), TEM image (D) and HRTEM image (E) of 2D/2D heterostructured g-C_3N_4/MnO_2, HRTEM image of the lattice spacing of MnO_2 NSs (F), EDX elemental mapping images (G-I) of 2D/2D heterostructured g-C_3N_4/MnO_2.

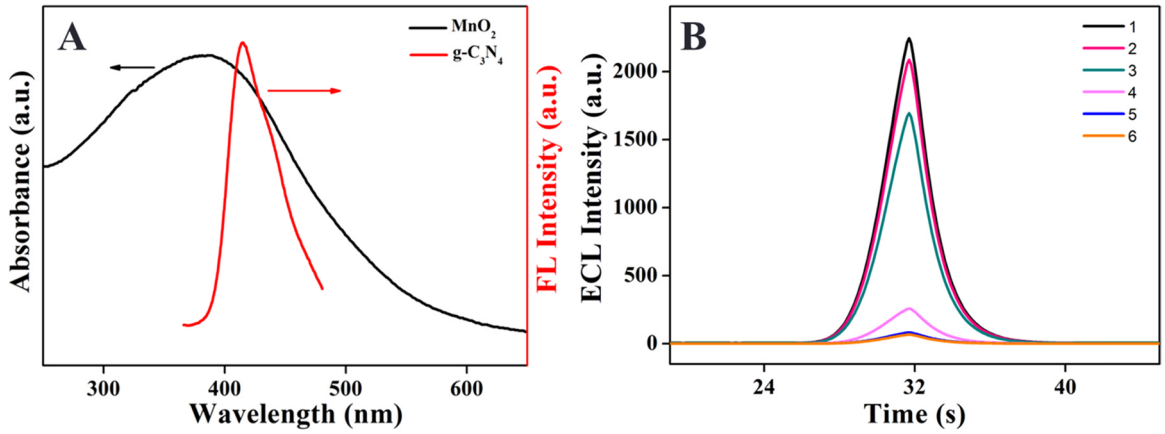

Fig. 3. (A) UV–vis absorption spectrum of MnO_2 NSs (black) and fluorescence emission spectrum of g-C_3N_4 NSs (red); (B) The ECL intensity-time curves of g-C_3N_4 (curve 1), g-C_3N_4 and GSH (curve 2), g-C_3N_4/MnO_2 and GSH (curve 3), g-C_3N_4/MnO_2 (curve 4), MnO_2 (curve 5), blank solution (curve 6).

3.3. Characterization of the designed "off-on" ECL sensing platform

Fig. 3B illustrated the ECL responses of different substances in the solution. The single g-C_3N_4 NSs emitted a strong cathodic ECL signal (curve 1). After formation of 2D/2D heterostructured g-C_3N_4/MnO_2 (curve 4), the ECL intensity emerged a dramatic decline, which could be resulted from the occurrence of ECL-RET between g-C_3N_4 and MnO_2. The appearance of GSH triggered the reduction of MnO_2 into Mn^{2+}, destroying the ECL-RET and further leading to the recovery of ECL intensity (curve 3).

3.4. Optimization of conditions

In order to realize the fine performance of the fabricated sensor, the pH and concentration of $K_2S_2O_8$ were optimized. As shown in Fig. S3A, with the change of pH from 6.0 to 9.0, the ECL intensity increased gradually and reached the maximum at 7.5, and then began to decrease. So, pH 7.5 was chosen. The influence of $K_2S_2O_8$ concentration was presented in Fig. S3B. The ECL intensity increased along with the increasing of $K_2S_2O_8$ concentration in range of 0.04–0.16 M. When the concentration exceeded 0.10 M, the intensity was slow down and then reached equilibrium. So, 0.10 M was used in the experiments. As a control, the ECL intensities of g-C_3N_4/MnO_2 in the different pH values and different $K_2S_2O_8$ concentrations without GSH were also evaluated, which were depicted in Fig. S4.

3.5. Analytical performance of sensing platform

The ECL responses of 2D/2D heterostructured g-C_3N_4/MnO_2 towards various concentrations of GSH were studied. As depicted in Fig. 4A, the ECL signals enhanced accompanied by the increment of the GSH concentration. This can be attributed to that the more GSH reduced more MnO_2, resulting in the release of g-C_3N_4 from the heterostructure and the recovery of ECL intensity. Fig. 4B exhibited that the ECL intensity is in direct proportion to the logarithmic concentration of GSH ranged from 0.2 μM to 100 μM. The regression equation is $I = 674.1 + 508.9 \log C$ (μM) with the correlation coefficient of 0.997. The limit of detection (LOD) for GSH was experimentally found as 0.05 μM. Furthermore, comparison with some reported methods (Table S1), the as-prepared ECL-RET platform shows good analytical performances.

3.6. Specificity, stability and reproducibility of the ECL sensor

To estimate the specificity of the ECL sensor toward GSH (100 μM), the ECL intensities of some ions (K^+, Mg^{2+}, Ca^{2+}, Cu^{2+}, Fe^{2+}, Fe^{3+}

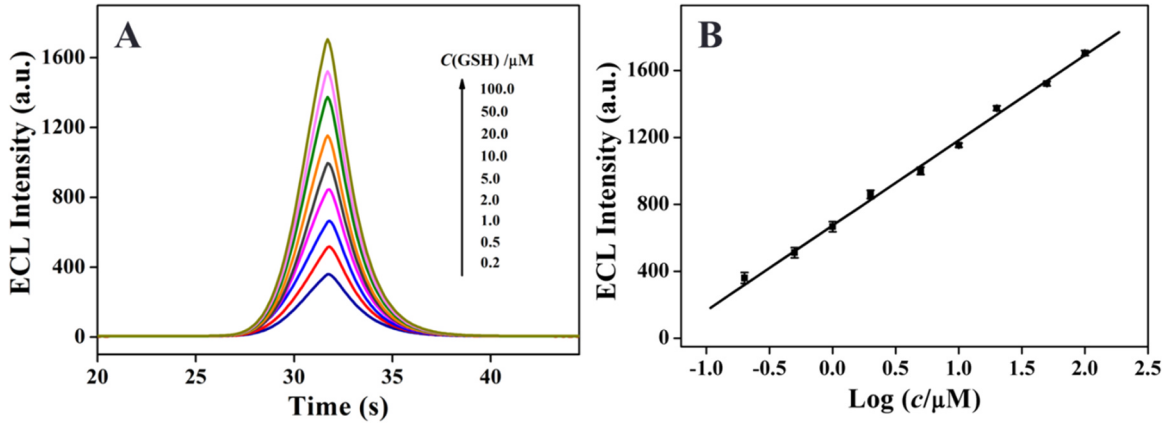

Fig. 4. (A) The ECL intensity-time curves and (B) the calibration curve of the fabricated sensor for GSH detection.

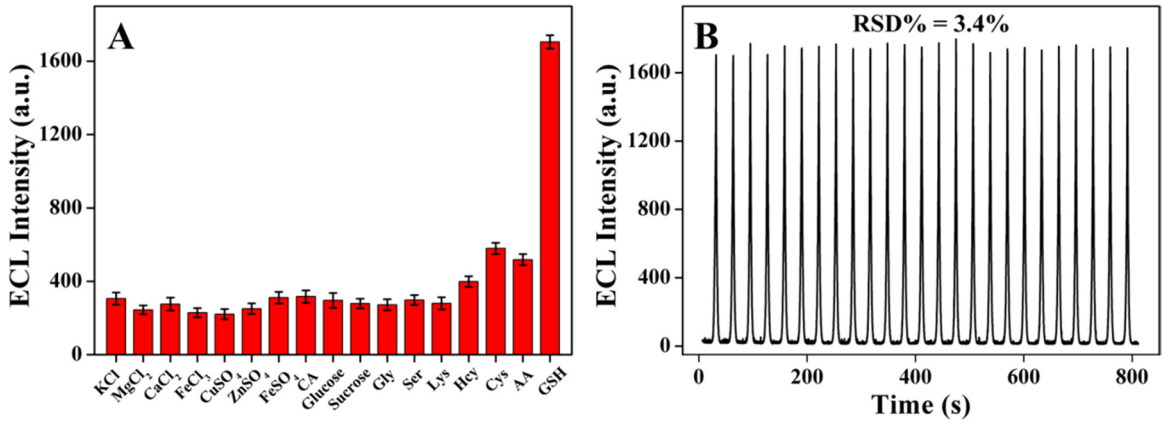

Fig. 5. (A) Selectivity and (B) stability of the ECL intensity of sensor.

and Zn^{2+}), amino acids (Gly, Ser, Lys, Hcy and Cys), saccharide (glucose and sucrose), CA and AA were tested. The results in Fig. 5A demonstrated that the addition of the interferents (each of 1000 μM) caused tiny ECL changes except Hcy, Cys and AA (each of 10.0 μM). Although the high concentrations of Hcy, Cys and AA also can produce ECL response in the system, their content (μM levels) is much lower than that of GSH (mM levels) in biological systems (Cai et al., 2015; Gao et al., 2016). For further evaluating the specificity of the sensor, the competitive experiments for detecting GSH in the presence of interferents mentioned above were performed, which were shown in Fig. S5. The results suggested that the presence of such interferents has little influence on GSH detection. Therefore, it can be concluded that this ECL sensor has the good selectivity for GSH detection.

The stability of the ECL sensor was investigated by continuous cyclic scans of the ECL sensor for 100 μM GSH (Fig. 5B). The ECL intensity remained nearly constant with the relative standard deviation (RSD) of 3.4%, which indicate the favorable stability of the ECL sensor.

In addition, to study the reproducibility of the ECL sensor, same batches (intra-assay) and different batches (inter-assay) of five sensors were taken. For 100 μM GSH, the RSDs of intra-assay and inter-assay were 4.9% and 6.1%, respectively. These results suggested an acceptable precision of the proposed system.

3.7. Real sample analysis

To test the practicability of the ECL sensor, the GSH content in human serums was measured. The recoveries were studied by adding the given amount of GSH (0.01, 1.00, 10.0 μM) into the pretreated human serum samples with 100-fold dilution. As listed in Table S2, the recoveries varied in the range of 87.0–112.0% and the RSDs were no more than 6.6%. Apparently, the satisfactory results made it feasible to apply the ECL sensor to the biology system.

4. Conclusions

In summary, a high-efficient ECL-RET system in 2D/2D heterostructured g-C_3N_4/MnO_2 was developed for the sensitive detection of GSH. Compared with most of the previous ECL-RET strategies, integrating the donor (g-C_3N_4 NSs) and acceptor (MnO_2 NSs) into one heterostructure greatly enhanced the RET efficiency as a consequence of shortened distance of donor–acceptor pair. To proof the performance of the ECL-RET system, the “off-on-type” ECL biosensor for GSH was designed and exhibited a low LOD of 0.05 μM and wide linear range of 0.2–100 μM. The applicability of the proposed method was also validated by the determination of GSH in human serum. We envision that such an ECL-RET in one heterostructure would provide promising perspective for constructing high efficient ECL-RET biosensing platforms.

CRediT authorship contribution statement

Xiao-Long Fu: Conceptualization, Methodology, Investigation, Writing - original draft. **Fang Hou:** Investigation. **Fu-Rao Liu:** Investigation. **Shu-Wei Ren:** Validation. **Jun-Tao Cao:** Conceptualization, Methodology, Project administration, Writing - original draft, Writing - review & editing. **Yan-Ming Liu:** Conceptualization, Methodology, Supervision, Project administration, Writing - original draft, Writing - review & editing.

Acknowledgements

This work was supported by the National Natural Science Foundation of China (Grant 21874115 and 21675136), Plan for Scientific Innovation Talent of Henan Province (2017JR0016), Science & Technology Innovation Talents in Universities of Henan Province (18HASTIT003), and Nanhu Young Scholar Supporting Program of XYNU.

Declaration of interests

The authors declare that they have no known competing financial interests or personal relationships that could have appeared to influence the work reported in this paper.

Appendix A. Supporting information

Supplementary data associated with this article can be found in the online version at doi:10.1016/j.bios.2019.01.010.

References

Babamiri, B., Salimi, A., Hallaj, R., 2018. Biosens. Bioelectron. 102, 328–335.
Cai, Q.Y., Li, J., Ge, J., Zhang, L., Hu, Y.L., Li, Z.H., Qu, L.B., 2015. Biosens. Bioelectron. 72, 31–36.
Cao, J.T., Wang, Y.L., Zhang, J.J., Dong, Y.X., Liu, F.R., Ren, S.W., Liu, Y.M., 2018. Anal. Chem. 90 (17), 10334–10339.
Chen, C.Y., Liu, W., Xu, C., Liu, W.S., 2015. Biosens. Bioelectron. 71, 68–74.
Chen, L.C., Huang, D.J., Ren, S.Y., Dong, T.Q., Chi, Y.W., Chen, G.N., 2013. Nanoscale 5 (1), 225–230.
Chen, M.M., Wang, Y., Cheng, S.B., Wen, W., Zhang, X.H., Wang, S.F., Huang, W.H., 2018. Anal. Chem. 90 (8), 5075–5081.
Cheng, C.M., Huang, Y., Tian, X.Q., Zheng, B.Z., Li, Y., Yuan, H.Y., Xiao, D., Xie, S.P., Choi, M.M.F., 2012. Anal. Chem. 84 (11), 4754–4759.
Clapp, A.R., Medintz, I.L., Mauro, J.M., Fisher, B.R., Bawendi, M.G., Mattoussi, H., 2004. J. Am. Chem. Soc. 126 (1), 301–310.
Dong, Y.P., Gao, T.T., Zhou, Y., Zhu, J.J., 2014. Anal. Chem. 86 (22), 11373–11379.
Feng, Y.Q., Wang, Q.B., Lei, J.P., Ju, H.X., 2015. Biosens. Bioelectron. 73, 7–12.
Gao, W.Y., Liu, Z.Y., Qi, L.M., Lai, J.P., Kitte, S.A., Xu, G.B., 2016. Anal. Chem. 88 (15), 7654–7659.
Hao, N., Li, X.L., Zhang, H.R., Xu, J.J., Chen, H.Y., 2014. Chem. Commun. 50 (94), 14828–14830.
Harfield, J.C., Batchelor-McAuley, C., Compton, R.G., 2012. Analyst 137 (10),

2285–2296.
Ji, J., He, L., Shen, Y.Y., Hu, P.P., Li, X.H., Jiang, L.P., Zhang, J.R., Li, L.L., Zhu, J.J., 2014. Anal. Chem. 86 (7), 3284–3290.
Ji, X., Wang, W.T., Mattoussi, H., 2016. Nano Today 11 (1), 98–121.
Ke, H., Sha, H.F., Wang, Y.F., Guo, W.W., Zhang, X., Wang, Z.M., Huang, C.S., Jia, N.Q., 2018. Biosens. Bioelectron. 100, 266–273.
Lei, Y.M., Huang, W.X., Zhao, M., Chai, Y.Q., Yuan, R., Zhuo, Y., 2015. Anal. Chem. 87 (15), 7787–7794.
Li, Z.Y., Lin, Z.F., Wu, X.Y., Chen, H.T., Chai, Y.Q., Yuan, R., 2017. Anal. Chem. 89 (11), 6029–6035.
Liu, J.Q., He, X.X., Wang, K.M., He, D.G., Wang, Y.H., Mao, Y.F., Shi, H., Wen, L., 2015. Biosens. Bioelectron. 70, 54–60.
Liu, Y.T., Wang, Q.B., Lei, J.P., Hao, Q., Wang, W., Ju, H.X., 2014. Talanta 122, 130–134.
Ma, H.M., Li, X.J., Yan, T., Li, Y., Liu, H.Y., Zhang, Y., Wu, D., Du, B., Wei, Q., 2016. ACS Appl. Mater. Interfaces 8 (16), 10121–10127.
Ngamchuea, K., Batchelor-McAuley, C., Compton, R.G., 2017. Anal. Chem. 89 (5), 2901–2908.
Niu, W.J., Zhu, R.H., Cosnier, S., Zhang, X.J., Shan, D., 2015. Anal. Chem. 87 (21), 11150–11156.
Peng, L.C., Zhang, P., Chai, Y.Q., Yuan, R., 2017. Anal. Chem. 89 (9), 5036–5042.
Qian, J., Wang, C.Q., Pan, X.H., Liu, S.Q., 2013. Anal. Chim. Acta 763, 43–49.
Sakai, N., Ebina, Y., Takada, K., Sasaki, T., 2005. J. Phys. Chem. B 109 (19), 9651–9655.
Sezgintürk, M.K., Dinçkaya, E., 2004. Biosens. Bioelectron. 19 (8), 835–841.
Tian, J.Q., Liu, Q., Asiri, A.M., Al-Youbi, A.O., Sun, X.P., 2013. Anal. Chem. 85 (11), 5595–5599.
Wang, J., Shan, Y., Zhao, W.W., Xu, J.J., Chen, H.Y., 2011. Anal. Chem. 83 (11), 4004–4011.
Wang, Y.L., Liu, F.R., Cao, J.T., Ren, S.W., Liu, Y.M., 2018. Biosens. Bioelectron. 102, 525–530.
Wang, Y.Z., Hao, N., Feng, Q.M., Shi, H.W., Xu, J.J., Chen, H.Y., 2016. Biosens. Bioelectron. 77, 76–82.
Wu, M.S., He, L.J., Xu, J.J., Chen, H.Y., 2014. Anal. Chem. 86 (9), 4559–4565.
Yin, J., Kwon, Y., Kim, D., Lee, D., Kim, G., Hu, Y., Ryu, J.H., Yoon, J., 2014. J. Am. Chem. Soc. 136 (14), 5351–5358.
Yu, H.L., Zheng, L., 2016. Microchim. Acta 183 (7), 2229–2234.
Yuan, Y.X., Wu, S.F., Shu, F., Liu, Z.H., 2014. Chem. Commun. 50 (9), 1095–1097.
Zhang, H., Zuo, F.M., Tan, X.R., Xu, S.H., Yuan, R., Chen, S.H., 2018. Biosens. Bioelectron. 104, 65–71.
Zhang, X.D., Xie, X., Wang, H., Zhang, J.J., Pan, B.C., Xie, Y., 2012. J. Am. Chem. Soc. 135 (1), 18–21.
Zhang, X.L., Zheng, C., Guo, S.S., Li, J., Yang, H.H., Chen, G.N., 2014. Anal. Chem. 86 (7), 3426–3434.